Three-phase four-wire shunt hybrid active power filter model with model predictive control in imbalance distribution networks

Asep Andang[1,2], Rukmi Sari Hartati[1], I Bagus Gede Manuaba[1], I Nyoman Satya Kumara[1]
[1]Department of Electrical Engineering, Universitas Udayana, Bali, Indonesia
[2]Department of Electrical Engineering, Faculty of Engineering, Universitas Siliwangi, Tasikmalaya, Indonesia

Article Info

ABSTRACT

This paper presents a harmonic reduction and load imbalance model in a three-phase four-wire distribution network. This model uses a hybrid active power filter, a passive inductor and capacitor filter, and an active power filter in the form of a three-phase, four-leg connected grid inverter. The switching of the voltage source converter on this filter uses finite control set model predictive control (FCS-MPC). Control of this hybrid active power filter uses model predictive control (MPC) with a cost function, comparing the reference current and prediction current with mathematical modelling of the circuit. The reference current is taken from the load current by extracting dq, and the predicted current is obtained from the iteration of the voltage source converter (VSC) switching pattern. Each combination is compared with the reference current in the cost function to get the smallest error used as a power switching signal. Modelling was validated by using MATLAB Simulink. The simulation results prove a decrease in harmonics at a balanced load from 22.16% to 4.2% and at an unbalanced load, reducing the average harmonics to 4.74%. The simulation also decreases the load current imbalance in the distribution network. Reducing the current in the neutral wire from 62.01%-0.42% and 11.29-0.3 A.

Corresponding Author:

Asep Andang
Department of Electrical Engineering, Faculty of Engineering, Universitas Siliwangi
Tasikmalaya 46115, Indonesia
Email: andhangs@unsil.ac.id

1. INTRODUCTION

The load balance has rarely occurred in the electricity distribution grid, as most single-phase charges are connected with different power ratings and numbers, resulting in imbalance. This further causes a current flow on the neutral wire, leading to the overheating of the grid and transformer, reducing transmission capability, and increasing transmission losses [1], [2]. The unbalanced load generates a negative sequence component current in a three-phase four-wired system and develops a zero-sequence charge in the neutral wire. The imbalance analysis has been described by various methods [3], [4], such as the Buchholz theorem based on apparent power, developed and redefined for multiple sources and unbalanced power load conditions. This apparent power is defined by IEEE standard 2010, as the root of quadratic active power addition, with reactive and unbalanced watts [5].

Moreover, the load imbalance is reported to be corrected by using a compensator. This improvement is compensated for the grid's negative and zero sequence currents [1]. Passive compensation is reported to have used reactive components to eliminate those of zero-sequence current at unbalanced voltages. However,

it is only suitable for static loads [6], [7]. The static synchronous compensator (STATCOM) initially functions as voltage control and reactive compensation in power networks. Moreover, it mitigates unbalanced load [8], making it an active compensator. The current decomposition for this unbalanced load compensator uses the modified synchronous reference frame (SRF) [9], [10] and instantaneous reactive power theory (IRPT) modification methods [11], [12] with the switch control using space vector pulse width modulation (SVPWM) [13], [14].

The decomposition of unbalanced load currents is directly unable to use the SRF method because it depends on the suitable frequency for fundamental components. An additional SRF calculation using-ωt is required based on the negative sequence component analysis. This method is known as the decouple synchronous reference frame (DSRF) [15].

Improving electrical energy quality by reducing reactive power was carried out using power factor correction (PFC) [16], [17]. However, the decrease in power quality due to harmonics on the grid could be improved by using a power filter. Based on static and dynamic load conditions, the reduction is also conducted by using passive power filters (PPF) and active power filters (APF) [18], [19]. The APF, shunt hybrid active power filter (SHAPF), and current decomposition reduce harmonics, reactive power, and load imbalance. Also, the use of APF/SHAPF in load imbalance conditions is carried out, using hysteresis control [20], IRPT [21], [22], SRF [23], [24], and fuzzy [25], [26]. The harmonic currents in this study were reduced through SHAPF with model predictive control (MPC) at a balanced load in three-phased three and four wires [27] and discussed in a separate article. The contribution of this research is the implementation of finite control set model predictive control (FCS-MPC) on an inductor capacitor passive filter (LC)-connected hybrid power filter with varying non-linear loads and its ability to overcome load imbalances.

2.   RESEARCH METHOD
2.1.   Shunt hybrid active power filter

The proposed SHAPF consists of passive LC and active filters in a three-phase four-wired grid-connected inverter (GCI) Figure 1. The primary function of this SHAPF was to produce harmonic compensation currents when different phases were generated from the switching process, according to the load i_L. It is then observed to have produced a clean waveform from harmonics formed in (1).

$$i_s = i_L + i_f \tag{1}$$

In three-phase four-wire, neutral currents were produced when the load condition was balanced, as indicated in (2).
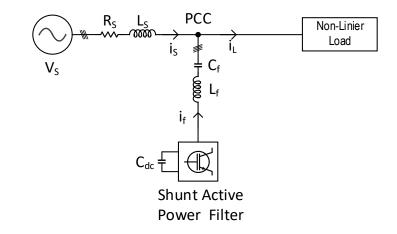
$$i_n = i_a + i_b + i_c \tag{2}$$

Figure 1. SHAPF circuit with LC

Based on (2), these forms of current flowing in the neutral wire (i_a, i_b, and i_c) were observed to have flowed through phases a, b and c. When the connected load condition was unbalanced, this value did not

equal zero. Therefore, this imbalance condition triggered a difference in the source voltage between the phases and the load current [28]. Furthermore, an adjustment was made to switching the power transistors on the active power filter, originating from the load's sampling process described in the reference current generation section. This adjustment was found to have been conducted to balance the load.

The installation of the LC filter at the neutral point is used in anticipating the presence of sequence currents that occur due to load imbalances. Besides that, the filter can smooth the ripples of the current wave. The selection of LC parameters in this circuit refers to tareen [29] and tang [30]; by using a ten times approach to the L_s system impedance as well as C, an approximation process is carried out based on reactive power requirements after which the experiment process is carried out.

2.2. Reference current generation

In this process, the decomposition of the load current is carried out to obtain the reference current. The reference current will be used as one of the control components to turn on the transistor as a switch on the hybrid filter. The process of generating this reference current used the SRF method, shown in Figure 2. This SRF method required input from the i_{La}, i_{Lb}, and i_{Lc} loads, in order to produce quadrature and direct axis currents (i_q and i_d) via the use of park transformation [31] as indicated in (3).

$$\begin{bmatrix} i_{Ld} \\ i_{Lq} \\ i_{L0} \end{bmatrix} = \frac{2}{3} \begin{bmatrix} sin(\omega t) & sin\left(\omega t - \frac{2\pi}{3}\right) & sin\left(\omega t + \frac{2\pi}{3}\right) \\ cos(\omega t) & cos\left(\omega t - \frac{2\pi}{3}\right) & cos\left(\omega t + \frac{2\pi}{3}\right) \\ \frac{1}{2} & \frac{1}{2} & \frac{1}{2} \end{bmatrix} \begin{bmatrix} i_{La} \\ i_{Lb} \\ i_{Lc} \end{bmatrix} \tag{3}$$

The sine and cos signals ω were obtained from the phase locked loop (PLL) process, with the source voltage as input [32]. This transformation process produced i_d, i_q, and i_0. The i_d was observed to consist i_d (dc) and i_d (ac), which were the fundamental and harmonic components of the load in the dq reference frames, as indicated in (4).

$$\left.\begin{array}{l} i_d = i_{d(dc)} + i_{d(ac)} \\ i_q = i_{q(dc)} + i_{q(ac)} \end{array}\right\} \tag{4}$$

Furthermore, the separation of harmonic currents on the d axis was carried out by pairing the low pass filter (LPF) to pass the i_d current in the fundamental system i_d (dc). i_d (ref) is obtained from subtracting i_d with $_{id\ (dc)}$, which is the result of the LPF process, and the output of this reduction is corrected by i_{dc}. For i_q, the conversion was carried out by reversing the phase, as indicated in (5). The reference signals i_d (ref), i_q (ref), and i_0 (ref) were converted into switching currents I_{La}^*, I_{Lb}^*, and I_{Lc}^*, via the use of (6).

$$i_{q(ref)} = -i_q \tag{5}$$

$$\begin{bmatrix} I_{La}^* \\ I_{Lb}^* \\ I_{Lc}^* \end{bmatrix} = \begin{bmatrix} sin(\omega t) & cos(\omega t) & 1 \\ sin\left(\omega t - \frac{2\pi}{3}\right) & cos\left(\omega t - \frac{2\pi}{3}\right) & 1 \\ sin\left(\omega t + \frac{2\pi}{3}\right) & cos\left(\omega t + \frac{2\pi}{3}\right) & 1 \end{bmatrix} \begin{bmatrix} i_{d(ref)} \\ i_{q(ref)} \\ i_{0(ref)} \end{bmatrix} \tag{6}$$
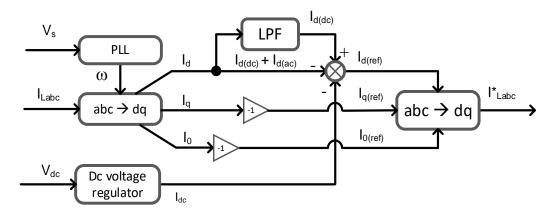

Figure 2. dq reference current generation

2.3. Model predictive control

In this SHAPF, the function of MPC was to control the switching of the four-leg inverter. The MPC started from the input current, $i_{La}^*c(k)$, which was then extrapolated through the third-order lagrange method [33] in order to produce $i_{ref}(k+1)$, as indicated in (7). Afterwards, this extrapolated output stream was inputted into the cost function.

$$i_{ref}(k+1) = 4i_{Labc}^*(k) - 6i_{Labc}^*(k-1) + 4i_{Labc}^*(k-2) - i_{Labc}^*(k-3) \tag{7}$$

The components $i_{Labc}^*(k)$, $i_{Labc}^*(k-1)$, $i_{Labc}^*(k-2)$ and $i_{Labc}^*(k-3)$, where the number of reference currents at time t=k, k-1, k-2, and k-3, respectively, where the sample period was 50 μs.

The prediction model was then built in (8), a closed-loop circuit.

$$v_{pccx} = L_f \frac{di}{dt} + R_f i + \frac{1}{C_f} \int idt + v_{inv} \tag{8}$$

v$_{pccx}$ was the point of common coupling (PCC) voltage in phase x. However, v$_{inv}$ was observed as the inverter voltage, S$_a$, S$_b$, S$_c$, and S$_d$, with v$_{dc}$ (input voltage). Also, L$_f$, R$_f$, and C$_f$ represented the inductance, resistance, and capacitance of the PPF. Moreover, (8) was then discretized for the derivative, using (9) and (10) for integration via the forward Euler.

$$\frac{di}{dt} \approx \frac{i(k+1)-i(k)}{T_s} \tag{9}$$

$$\frac{1}{C_f} \int idt = \frac{T_s}{C_f}\left(i(k+1) + i(k)\right)I \tag{10}$$

Afterwards, (8) was rearranged by (9) and (10) with inputs, which were in the form of v$_{dc}$ (DC voltage), i$_f$(k) (filter current), and the output voltage of the inverter v$_{inv}$, in order to produce i$_{pre}$ (k+1), as indicated in (11).

$$i(k+1) = \frac{1}{\left(\frac{L_f}{T_s}+R_f+\frac{T_s}{C_f}\right)}\left(v_{pccx} - v_{inv} - \left(\frac{T_s}{C_f} - \frac{L_f}{T_s}\right)\left(i(k)\right)\right) \tag{11}$$

The resulting extrapolated and prediction model currents, I$_{ref}$(k+1) and I$_{pre}$(k+1), were then compared in order to make observations based on the 16 switching conditions of I$_{pre}$(k+1), which approached I$_{ref}$(k+1). Therefore, the slightest difference between i(k+1) and I$_{pre}$(k+1) with that particular switching condition was used in the system.

2.4. Unbalanced load

When an unbalanced non-linear load was connected to a four-wire three-phase distribution grid, the system became imbalanced and produced symmetrical components from positive, negative, and zero sequences. Moreover, decomposition analysis was carried out via the Fortescue transformation, as indicated in (12) [34]:

$$\begin{bmatrix} i_a \\ i_b \\ i_c \end{bmatrix} = \begin{bmatrix} 1 & 1 & 1 \\ 1 & a & a^2 \\ 1 & a^2 & a \end{bmatrix}\begin{bmatrix} i_0 \\ i_1 \\ i_2 \end{bmatrix} \tag{12}$$

where a=1∠120°, i$_0$, i$_1$, i$_2$ is the zero, positive, and negative symmetric sequence components. Afterwards, (12) was inputted into (3) to determine the number of negative sequence currents. Therefore, these negative sequence currents were eliminated in order for the load conditions to be balanced. In order to determine the hugeness of the current imbalance, which was measured by (14), Patel's method was carried out [35].

$$K_{ir} = \frac{i_2}{i_1} \tag{13}$$

$$\%I_{unb} = \frac{|I_{a,rms}-I_{b,rms}|+|I_{b,rms}-I_{c,rms}|+|I_{c,rms}-I_{a,rms}|}{I_{a,rms}+I_{b,rms}+I_{c,rms}} x100 \tag{14}$$

3.   RESULTS AND DISCUSSION

Simulations were carried out on a three-phase four-wired electricity distribution grid, using a PCC voltage of V_s=400 volts, with a fundamental frequency, inductance, and resistance of f_0=50 Hz, L_s=5 mH, and R_s=0.001 Ω, respectively. Moreover, the grid-connected and unbalanced non-linear load. Simulation to test modelling using MATLAB/Simulink. The first test was carried out with a single-phase rectifier load connected to each resistor and inductor (RL) load to represent a balanced loading condition. Afterwards, the second test was non-linear with unbalanced loads in one phase. Furthermore, each phase's third simulation was carried out with different loads to represent three-phase imbalanced loading. This simulation model is presented in Figure 3.
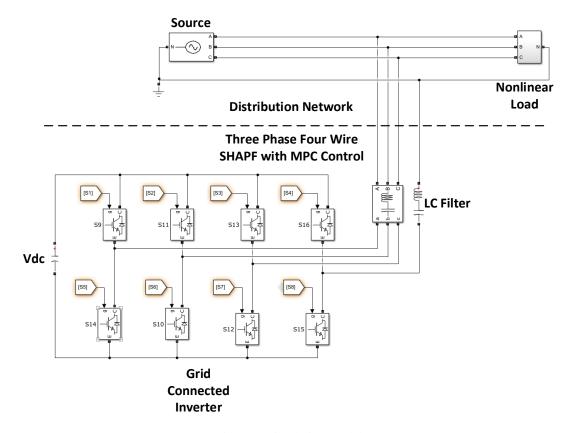
Figure 3. Simulation model

3.1. Simulation on balanced load

The simulation is performed using a balanced load. This balanced load takes the form of a single-phase rectifier circuit connected to a resistor and an inductor, as shown in Figure 4. The value of this load parameter is shown in Table 1.
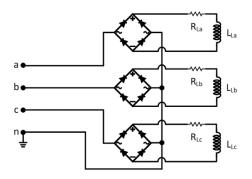
Figure 4. Load circuit

The results of the load voltage experienced distortion, as indicated in Figure 5(a), with the source current resulting in total harmonics distortion of source current (THDi) and average root mean square (RMS) values of 22.16% and 11.6 A, which were presented in 5(b). The SHAPF installation on the balanced load succeeded in reducing the harmonic current so that the THDi became 4.2%. The current waveform can be seen in Figure 5(c).

Table 1. Load parameter

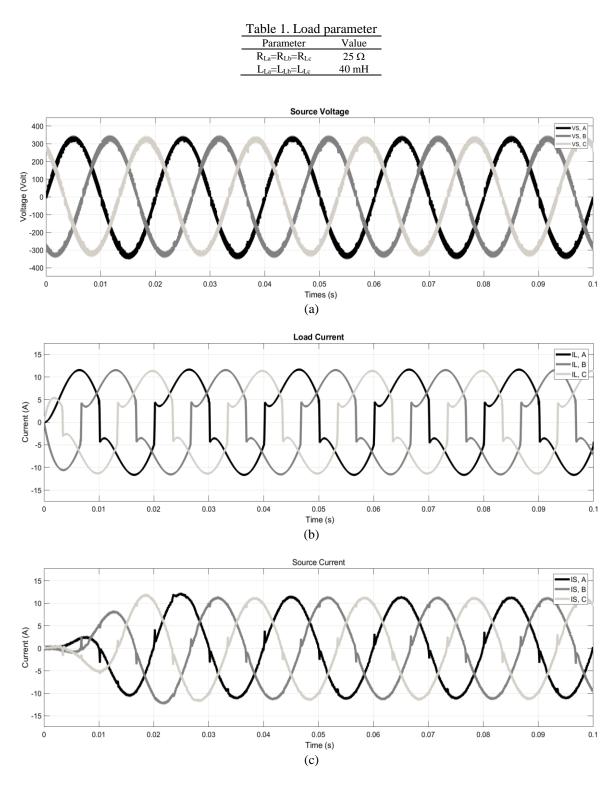| Parameter	Value
$R_{La}=R_{Lb}=R_{Lc}$	25 Ω
$L_{La}=L_{Lb}=L_{Lc}$	40 mH

(a)

(b)

(c)

Figure 5. Balanced load test result waveform (a) PCC voltage, (b) load current without SHAPF, and (c) load current with SHAPF

The balanced non-linear load simulation results showed a significant reduction in THD and neutral current, with small ripples. The reference current generated by each phase also had the same shape. The current wave spectrum can be seen in Figure 6(a) there is a significant decrease, especially low-order harmonics, to below 2%, while the voltage wave spectrum can be seen in Figure 6(b) changes do not occur significantly due to the FCS-MPC process in the cost function does not involve the voltage equation as part of the GCI switching pattern. Figure 7(a) shows the current harmonic wave spectrum before SHAP installation, where the current waveform is not purely sinusoidal, while in Figure 7(b), there is a change in the current waveform due to a decrease in THD.
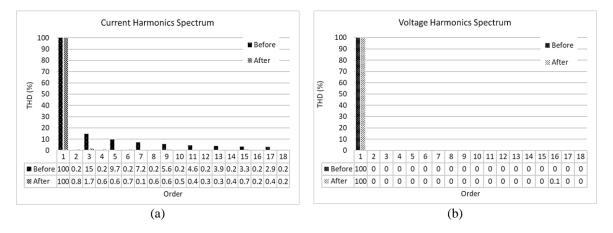

| | (a) | | (b) |

Figure 6. Harmonic spectrum (a) current spectrum and (b) voltage spectrum
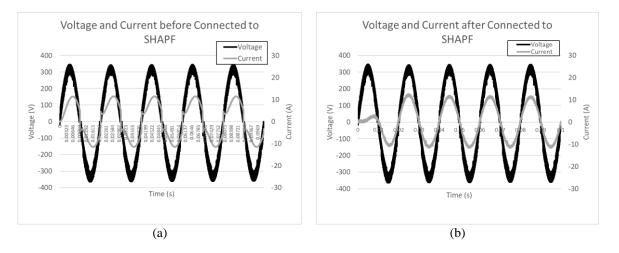

| | (a) | | (b) |

Figure 7. Voltage and load current waveform (a) before installation of SHAPF and (b) after installation of SHAPF

3.2. Simulation on unbalanced load

Based on the unbalanced load simulation, the circuit is shown in Figure 4, with the test being carried out by changing the load parameter, as indicated in Table 2. The waveform of the simulation results for the load current is presented in Figure 8(a). As a result of this load imbalance, a different measured RMS current value was produced using (14). However, the THD of the different load phases also experienced a difference in value, with $THDi_a$, $THDi_b$, and $THDi_c$ at 21.95%, 39.72%, and 21.80%, respectively. By having the same RMS current for phases, a and c at 11.63 amperes, the value of b is 20.33 amperes; from Patel (14), we get the current imbalance %Iunb=39.9%. The installation of SHAPF on the PCC side resulted in a decrease in THDi that occurred in $THDi_a$, $THDi_b$, and $THDi_c$ by 3.31%, 5.65%, and 3.36%, respectively. The installation of SHAPF succeeded in reducing the %Iunb load imbalance through (14), from 39.96% to 0.94%. The current waveform of the harmonic reduction is shown in Figure 8(b). The current harmonic spectrum can be seen in Figure 9(a), while the voltage harmonic spectrum can be seen in Figure 9(b).

Table 2. Load parameter

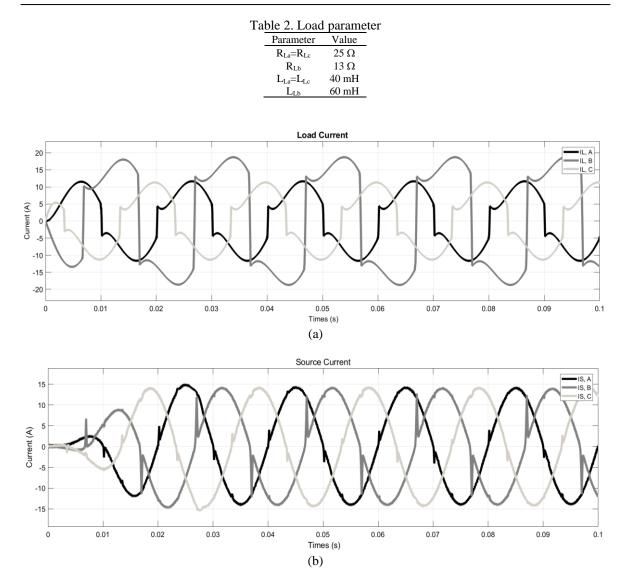| Parameter	Value
$R_{La}=R_{Lc}$	25 Ω
R_{Lb}	13 Ω
$L_{La}=L_{Lc}$	40 mH
L_{Lb}	60 mH

(a)

(b)

Figure 8. Unbalanced load simulation result waveform (a) current waveform without SHAPF and (b) current waveform with SHAPF
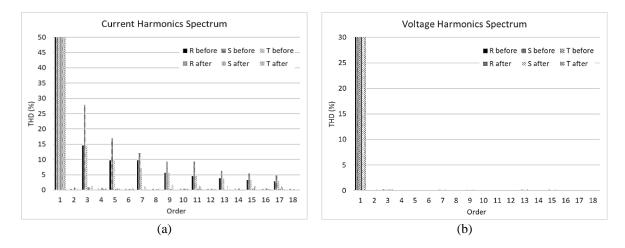

(a)

(b)

Figure 9. Harmonics spectrum under unbalanced load (a) current harmonics spectrum and (b) voltage harmonics spectrum

The load imbalance was also observed to have caused a neutral current flow. The simulation also showed a decrease in the RMS neutral current from 6.137 to 0.2 A. The neutral current waveform before and after the installation of SHAPF was presented in Figures 10(a) and 10(b).
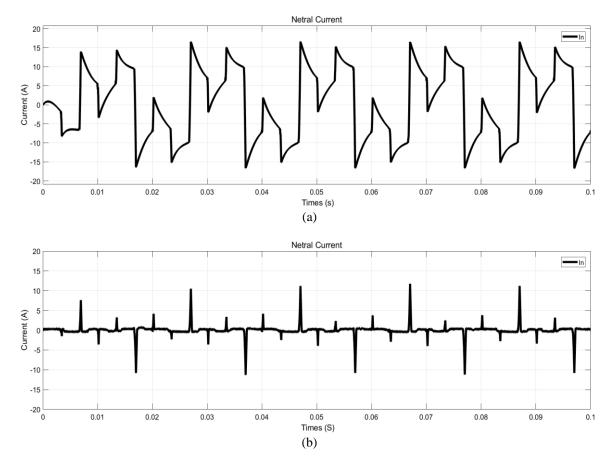

(a)

(b)

Figure 10. Neutral current at load on unbalanced load (a) without SHAPF and (b) with SHAPF

3.3. Simulation with different loads for each phase

This test is carried out with the topology in Figure 4, with each load having a different value, as shown in Table 3. The difference in each phase's load produced a loaded waveform with different harmonics and RMS values of i_a, i_b, and i_c, at 11.62, 20.37, and 7.98 A, respectively. The waveform of the imbalance current is presented in Figure 11(a). A calculation based on (14) found that % Iunb was 62.01%, with $THDi_a$, $THDi_b$, and $THDi_c$, 21.61%, 39.08%, and 18.62%, respectively.

The harmonic reduction process that occurs at an unbalanced load is presented in Figure 11(b). The THD reduction process is still running normally, even though the simulated load does not match the SHAPF rating. There was also a decrease in the current imbalance % I_{unb} by 0.42% and THD to an average of 4.74%. This load imbalance produces a neutral current of 11.29 A. After the hybrid power filter is installed, the neutral current becomes 0.3 A. The current waveforms before and after the installation of SHAPF are represented in Figures 12(a) and 12(b), while the current harmonic spectrum can be seen in Figure 13(a), and the voltage harmonic spectrum can be seen in Figure 13(b).

Table 3. Load parameter

Parameter	Value
R_{La}	25 Ω
R_{Lb}	13 Ω
R_{Lc}	37 Ω
L_{La}	40 mH
L_{Lb}	60 mH
L_{Lc}	50 mH

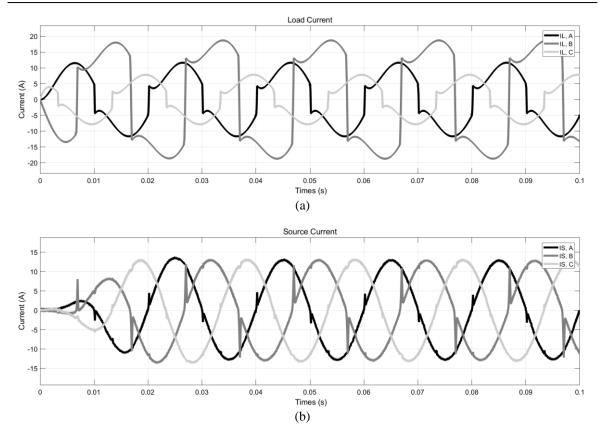*Three-phase four-wire shunt hybrid active power filter model … (Asep Andang)*

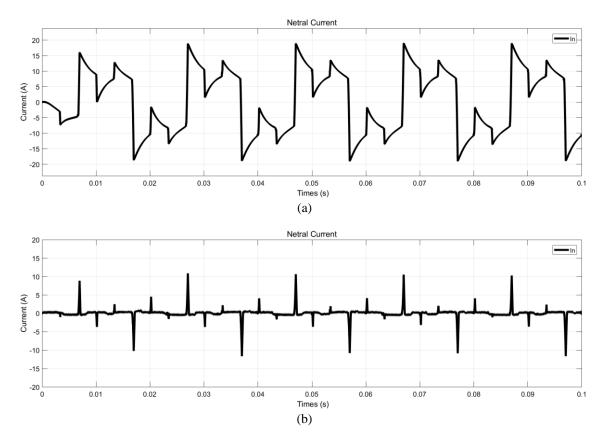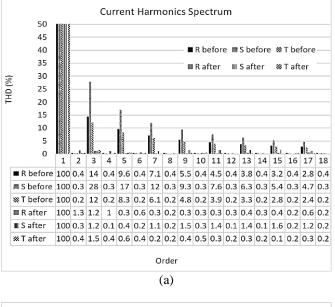Figure 11. The current waveform at different loads for each phase (a) without SHAPF and (b) with SHAPF

Figure 12. Neutral current on different loads for each phase (a) without SHAPF and (b) with SHAPF
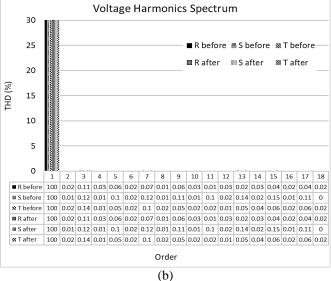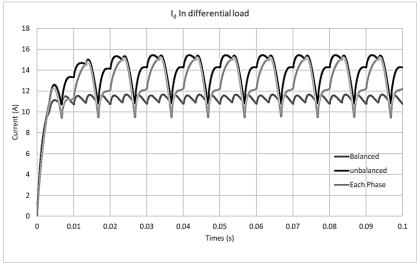
Current Harmonics Spectrum

Order	1	2	3	4	5	6	7	8	9	10	11	12	13	14	15	16	17	18
■ R before	100	0.4	14	0.4	9.6	0.4	7.1	0.4	5.5	0.4	4.5	0.4	3.8	0.4	3.2	0.4	2.8	0.4
▦ S before	100	0.3	28	0.3	17	0.3	12	0.3	9.3	0.3	7.6	0.3	6.3	0.3	5.4	0.3	4.7	0.3
▨ T before	100	0.2	12	0.2	8.3	0.2	6.1	0.2	4.8	0.2	3.9	0.2	3.3	0.2	2.8	0.2	2.4	0.2
■ R after	100	1.3	1.2	1	0.3	0.6	0.3	0.2	0.3	0.3	0.3	0.3	0.4	0.3	0.4	0.2	0.6	0.2
▥ S after	100	0.3	1.2	0.1	0.4	0.2	1.1	0.2	1.5	0.3	1.4	0.1	1.4	0.1	1.6	0.2	1.2	0.2
▨ T after	100	0.4	1.5	0.4	0.6	0.4	0.2	0.2	0.4	0.5	0.3	0.2	0.3	0.2	0.1	0.2	0.3	0.2

Order

(a)

Voltage Harmonics Spectrum

Order	1	2	3	4	5	6	7	8	9	10	11	12	13	14	15	16	17	18
■ R before	100	0.02	0.11	0.03	0.06	0.02	0.07	0.01	0.06	0.03	0.01	0.03	0.02	0.03	0.04	0.02	0.04	0.02
▦ S before	100	0.01	0.12	0.01	0.1	0.02	0.12	0.01	0.11	0.01	0.1	0.02	0.14	0.02	0.15	0.01	0.11	0
▨ T before	100	0.02	0.14	0.01	0.05	0.02	0.1	0.02	0.05	0.02	0.02	0.01	0.05	0.04	0.06	0.02	0.06	0.02
■ R after	100	0.02	0.11	0.03	0.06	0.02	0.07	0.01	0.06	0.03	0.01	0.03	0.02	0.03	0.04	0.02	0.04	0.02
▥ S after	100	0.01	0.12	0.01	0.1	0.02	0.12	0.01	0.11	0.01	0.1	0.02	0.14	0.02	0.15	0.01	0.11	0
▨ T after	100	0.02	0.14	0.01	0.05	0.02	0.1	0.02	0.05	0.02	0.02	0.01	0.05	0.04	0.06	0.02	0.06	0.02

Order

(b)

Figure 13. Harmonics spectrum under different load (a) current harmonics spectrum and (b) voltage harmonics spectrum
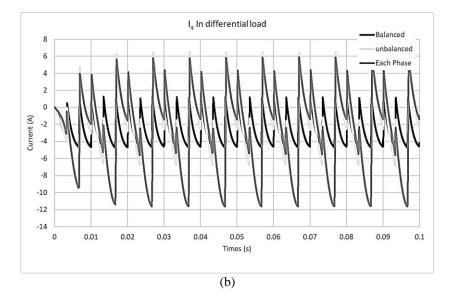
3.4. Discussion

The extraction of load currents to determine harmonics was carried out by the dq method to produce i_d and i_q components. In balanced loads, the i_d and i_q currents do not contain negative or zero symmetric sequence components. However, when the load was unbalanced, either one of the phases was not balanced, with i_d and i_q currents containing sequence components in negative and zero orders. The effect of the load imbalance on i_d and i_q currents was further illustrated in Figure 14.

Figure 14(a) shows that the current i_d produces a small ripple wave with no peak variation for a balanced load. However, one of the phases results in a more complicated curve for unbalanced loads. In addition, the waveform indicates load imbalance. Figure 14(b) shows that the current ripple for i_q at a balanced load is less than that at an unbalanced load, resulting in very different magnitudes between the two conditions. According to the neutral currents in Figure 14(c), even though the inrush charge is small for a balanced load, they still produce an i_0 signal. However, the magnitude of the observed current is enormous for an unbalanced load. In decomposing the symmetrical component for unbalanced loads, two SRF blocks were needed to anticipate the negative sequence's angular value and the opposite ωt. The resulting product was a better reference current, as it still reduced imbalances in this simulated study.
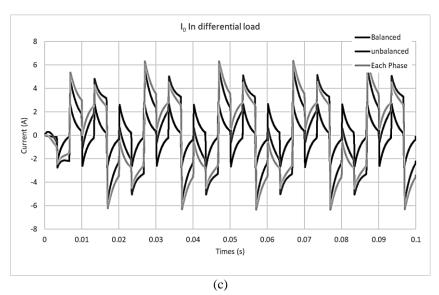
(a)

(b)

(c)

Figure 14. Extraction current in i_d, i_q, and i_0 (a) i_d with different load conditions, (b) i_q in different load conditions, and (c) i_0 in different load conditions

4.   CONCLUSION

This paper highlights how to mitigate harmonics in distribution networks at unbalanced loads. Harmonic mitigation is done by injecting the current generated from the converter switching process. This injection current is obtained by comparing the reference current and the predicted current in the cost function to produce a power switch ignition pattern. Unbalanced current decomposition using the SRF method could balance the load current and reduce harmonics. In the simulation results on MATLAB/Simulink, the harmonics at the balanced load can be reduced to comply with the IEEE 519-2014 standard. At unbalanced non-linear loads, where current flows in the neutral wire, the installation of a hybrid power filter can reduce the harmonics and, at the same time, reduce the current in the neutral wire so that the imbalance can be reduced. Therefore, this filter can be used at varying and unbalanced loads in each phase, especially in industrial use.

REFERENCES

[1]   R. Montoya-Mira, P. A. Blasco, J. M. Diez, R. Montoya, and M. J. Reig, "Unbalanced and reactive currents compensation in three-phase four-wire sinusoidal power systems," *Applied Sciences*, vol. 10, no. 5, Mar. 2020, doi: 10.3390/app10051764.

[2]   L. Wang, C.-S. Lam, and M.-C. Wong, "Unbalanced control strategy for a thyristor-controlled LC-coupling hybrid active power filter in three-phase three-wire systems," *IEEE Transactions on Power Electronics*, vol. 32, no. 2, pp. 1056–1069, Feb. 2017, doi: 10.1109/TPEL.2016.2555330.

[3]   V. León-Martínez, J. Montañana-Romeu, E. Peñalvo-López, and I. Valencia-Salazar, "Relationship between buchholz's apparent power and instantaneous power in three-phase systems," *Applied Sciences*, vol. 10, no. 5, Mar. 2020, doi: 10.3390/app10051798.

[4]   M. Artemenko, "New definition formulas for apparent power and active current of three-phase power system," *Przegląd Elektrotechniczny*, vol. 1, no. 8, pp. 83–87, Aug. 2019, doi: 10.15199/48.2019.08.20.

[5]   A. E. Emanuel, "Summary of IEEE standard 1459: Definitions for the measurement of electric power quantities under sinusoidal, nonsinusoidal, balanced, or unbalanced conditions," *IEEE Transactions on Industry Applications*, vol. 40, no. 3, pp. 869–876, 2004, doi: 10.1109/TIA.2004.827452.

[6]   P. A. Blasco, R. Montoya-Mira, J. M. Diez, R. Montoya, and M. J. Reig, "Compensation of reactive power and unbalanced power in three-phase three-wire systems connected to an infinite power network," *Applied Sciences*, vol. 10, no. 1, Dec. 2019, doi: 10.3390/app10010113.

[7]   L. R. Limongi, F. Bradaschia, C. H. de O. Lima, and M. C. C., "Reactive power and current harmonic control using a dual hybrid power filter for unbalanced non-linear loads," *Energies*, vol. 11, no. 6, May 2018, doi: 10.3390/en11061392.

[8]   H. Huang, L. Zhang, O. J. K. Oghorada, and M. Mao, "A delta-connected MMCC-based active power conditioner for unbalanced load compensation and harmonic elimination," *International Journal of Electrical Power and Energy Systems*, vol. 118, Jun. 2020, doi: 10.1016/j.ijepes.2019.105811.

[9]   Y. Yamamoto and T. Mannen, "Three-phase unbalance compensator using neutral point clamped multilevel interleaved inverter," in *2018 IEEE 4th Southern Power Electronics Conference (SPEC)*, Dec. 2018, pp. 1–7., doi: 10.1109/SPEC.2018.8636092.

[10]   P.-H. Wu, H.-C. Chen, Y.-T. Chang, and P.-T. Cheng, "Delta-connected cascaded H-bridge converter application in unbalanced load compensation," *IEEE Transactions on Industry Applications*, vol. 53, no. 2, pp. 1254–1262, Mar. 2017, doi: 10.1109/TIA.2016.2633945.

[11]   C. Yin, F. Wang, X. Ding, C. Tian, and P. Duan, "A novel compensator for three-phase load unbalance of the low voltage distribution network," in *2017 Chinese Automation Congress (CAC)*, Oct. 2017, pp. 7518–7521., doi: 10.1109/CAC.2017.8244138.

[12]   S. Jiao, R. Krishna, and K. Rajashekara, "A novel DROGI algorithm for non-linear unbalanced load compensation using four-leg converter," in *2020 IEEE Applied Power Electronics Conference and Exposition (APEC)*, Mar. 2020, pp. 3282–3286., doi: 10.1109/APEC39645.2020.9124133.

[13]   Z. Zhang and Y. Liu, "A novel unbalance loads compensation method based on ultra-capacitor," in *2018 IEEE International Power Electronics and Application Conference and Exposition (PEAC)*, Nov. 2018, pp. 1–5., doi: 10.1109/PEAC.2018.8590503.

[14]   A. K. Giri, S. Singh, R. Dash, R. Paul, S. C. Swain, and P. Panda, "A review on application of ANN and machine learning algorithm for the optimal placement of STATCOM," in *2019 Innovations in Power and Advanced Computing Technologies (i-PACT)*, Mar. 2019, pp. 1–5., doi: 10.1109/i-PACT44901.2019.8960138.

[15]   G. Ahrabian, F. Shahnia, and M. Haque, "Hybrid filter applications for power quality improvement of power distribution networks utilizing renewable energies," in *2006 IEEE International Symposium on Industrial Electronics*, Jul. 2006, pp. 1161–1165., doi: 10.1109/ISIE.2006.295801.

[16]   A. Ojo, K. Awodele, and A. Sebitosi, "Load compensation in a three-phase four wire distribution system considering unbalance, neutral current elimination and power factor improvement," in *2019 Southern African Universities Power Engineering Conference/Robotics and Mechatronics/Pattern Recognition Association of South Africa (SAUPEC/RobMech/PRASA)*, Jan. 2019, pp. 389–394., doi: 10.1109/RoboMech.2019.8704821.

[17]   M. M. Hashemipour and T.-L. Lee, "Integrated power factor correction and voltage fluctuation mitigation of microgrid using STATCOM," in *2017 IEEE 3rd International Future Energy Electronics Conference and ECCE Asia (IFEEC 2017-ECCE Asia)*, Jun. 2017, no. 3, pp. 1215–1219., doi: 10.1109/IFEEC.2017.7992215.

[18]   L. Gumilar, A. Kusumawardana, W. S. Nugroho, and M. Sholeh, "Power quality enhancement on hybrid power plants using shunt passive power filter and detuned reactor," in *2020 International Conference on Smart Technology and Applications (ICoSTA)*, Feb. 2020, pp. 1–6., doi: 10.1109/ICoSTA48221.2020.1570599090.

[19]   S. Puchalapalli and N. M. Pindoriya, "Study of control strategies for shunt active power filter for harmonics suppression," in *2017 7th International Conference on Power Systems (ICPS)*, Dec. 2017, pp. 218–223., doi: 10.1109/ICPES.2017.8387296.

[20] A. Teta, M. M. Rezaoui, A. Kouzou, A. A. Laouid, and S. Bensaoucha, "Analysis of reference current identification strategies for shunt active filter under distorted load conditions," in *2018 International Conference on Electrical Sciences and Technologies in Maghreb (CISTEM)*, Oct. 2018, pp. 1–6., doi: 10.1109/CISTEM.2018.8613346.

[21] T. Mahni, M. T. Benchouia, K. Srairi, A. Ghamri, and A. Golea, "Three-phase for-wire shunt active filter with unbalanced loads," *Energy Procedia*, vol. 50, pp. 528–535, 2014, doi: 10.1016/j.egypro.2014.06.064.

[22] M. Tali, A. Essadki, and T. Nasser, "Harmonic detection methods of shunt active power filter under unbalanced loads," in *2016 International Renewable and Sustainable Energy Conference (IRSEC)*, Nov. 2016, pp. 1017–1023., doi: 10.1109/IRSEC.2016.7984003.

[23] J. Yao, W. Zhu, L. Meng, H. Lin, Z. Shu, and L. Liu, "Unbalanced harmonic suppression of three-level active power filter with optimal hybrid control," in *2019 IEEE 10th International Symposium on Power Electronics for Distributed Generation Systems (PEDG)*, Jun. 2019, pp. 207–211., doi: 10.1109/PEDG.2019.8807494.

[24] P. Santiprapan, K. Areerak, and K. Areerak, "Proportional plus resonant control for active power filter in unbalanced system," in *2017 International Electrical Engineering Congress (iEECON)*, Mar. 2017, pp. 1–4., doi: 10.1109/IEECON.2017.8075733.

[25] R. Vlasenko, O. Bialobrzheskyi, and A. Gladyr, "Four-wire three-phase active power filter with fuzzy controller for compensation of distortion of currents unbalance in the conditions of fluctuated load," in *2019 IEEE International Conference on Modern Electrical and Energy Systems (MEES)*, Sep. 2019, pp. 222–225., doi: 10.1109/MEES.2019.8896448.

[26] H. Vanjani, U. K. Choudhury, M. Sharma, and B. Vanjani, "Takagi-sugeno (TS)-type fuzzy logic controller for three-phase four-wire shunt active power filter for unbalanced load," in *2016 IEEE 7th Power India International Conference (PIICON)*, Nov. 2016, pp. 1–4., doi: 10.1109/POWERI.2016.8077227.

[27] A. Andang, R. S. Hartarti, I. B. G. Manuaba, and I. N. S. Kumara, "Harmonics reduction on electric power grid using shunt hybrid active power filter with finite-control-set model-predictive control," *International Review on Modelling and Simulations (IREMOS)*, vol. 13, no. 1, Feb. 2020, doi: 10.15866/iremos.v13i1.17891.

[28] H. Arghavani and M. Peyravi, "Unbalanced current-based tariff," *CIRED-Open Access Proceedings Journal*, no. 1, pp. 883–887, Oct. 2017, doi: 10.1049/oap-cired.2017.0129.

[29] W. U. K. Tareen and S. Mekhielf, "Three-phase transformerless shunt active power filter with reduced switch count for harmonic compensation in grid-connected applications," *IEEE Transactions on Power Electronics*, vol. 33, no. 6, pp. 4868–4881, Jun. 2018, doi: 10.1109/TPEL.2017.2728602.

[30] X. Tang, Y. Wang, X. Zhang, W. Si, Y. Tao, and Z. Wang, "An overall optimization strategy for novel hybrid parallel active power filters based on genetic algorithm," in *Twenty-First Annual IEEE Applied Power Electronics Conference and Exposition, 2006. APEC '06.*, 2006, pp. 145–150., doi: 10.1109/APEC.2006.1620530.

[31] Y. Hoon, M. Mohd Radzi, M. Hassan, and N. Mailah, "DC-link capacitor voltage regulation for three-phase three-level inverter-based shunt active power filter with inverted error deviation control," *Energies*, vol. 9, no. 7, Jul. 2016, doi: 10.3390/en9070533.

[32] K. Kamel, Z. Laid, and K. Abdallah, "Mitigation of harmonics current using different control algorithms of shunt active power filter for non-linear loads," in *2018 International Conference on Applied Smart Systems (ICASS)*, Nov. 2018, pp. 1–4., doi: 10.1109/ICASS.2018.8652066.

[33] V. Yaramasu and B. Wu, *Model predictive control of wind energy conversion systems*. Hoboken: Wiley, 2017., doi: 10.1002/9781119082989.

[34] J. D. Glover, T. J. Overbye, and M. S. Sarma, *Power system analysis and design sixth edition*. 2017.

[35] A. Patel, H. D. Mathur, and S. Bhanot, "An improved control method for unified power quality conditioner with unbalanced load," *International Journal of Electrical Power and Energy Systems*, vol. 100, no. January, pp. 129–138, Sep. 2018, doi: 10.1016/j.ijepes.2018.02.035.

BIOGRAPHIES OF AUTHORS

Asep Andang [ID] [GS] [SC] [C] received a Master of Electrical Engineering from the Bandung Institute of Technology in 2006. He now works as a lecturer at the Department of Electrical Engineering at Siliwangi University in Tasikmalaya-Indonesia. He is currently a PhD candidate at Udayana University-Indonesia. His research interests include Power Quality, Power Electronics, and Drives, Internet of Things, and Automation. He can be contacted at email: andhangs@unsil.ac.id.

Rukmi Sari Hartarti [ID] [GS] [SC] [C] completed her undergraduate program at Sepuluh Nopember Institute of Technology (ITS), Surabaya-Indonesia in 1978. She then received a Master of Technology from Bandung Institute of Technology (ITB), Bandung, Indonesia in 1994 and Doctor of Philosophy from the University of Dalhousie-Canada in 2002. Currently, she is a Professor at the Department of Electrical Engineering at Udayana University. Her research interests include Power Quality and Power System Analysis, and System Optimization. She can be contacted at email: rukmisari@unud.ac.id.

I Bagus Gede Manuaba received a Bachelor's degree in Electrical Engineering from Udayana University in Denpasar-Indonesia, in 1996 and a Master in Electrical Engineering from the Institute of Technology Sepuluh Nopember (ITS), Surabaya-Indonesia, in 1999 and Doctoral degree in Electrical Engineering in 2016. He is a lecturer at Udayana University and has been working there since 1999. His research interests are Modeling and Power Plant Control, Operation, Optimization, and Intelligent Control Systems. He is also a member of The Institute of Electrical and Electronics Engineers (IEEE) since 2016. He can be contacted at email: ibgmanuaba@unud.ac.id.

I Nyoman Satya Kumara received a Bachelor's degree in Electrical Engineering from Udayana University, Denpasar-Indonesia in 1995, a Master in Electrical Power from the University of Newcastle upon Tyne in 1999, and a Ph.D. from Department of Electrical Electronic and Computer Engineering in the United Kingdom in 2006. His research interests include Renewable Energy Technology, Energy Management, Power Electronics, and Drive and Smart Systems. He can be contacted at email: satya.kumara@unud.ac.id.